ResearchGate

See discussions, stats, and author profiles for this publication at: https://www.researchgate.net/publication/228657375

Controllable Electrochemical Synthesis of Hierarchical ZnO Nanostructures on FTO Glass

ARTICLE *in* THE JOURNAL OF PHYSICAL CHEMISTRY C · AUGUST 2009

Impact Factor: 4.77 · DOI: 10.1021/jp902834j

CITATIONS
54

READS
34

6 AUTHORS, INCLUDING:

Lu Hong
Beihang University(BUAA)
189 PUBLICATIONS **2,740** CITATIONS
SEE PROFILE

Dai-Bin Kuang
Sun Yat-Sen University
111 PUBLICATIONS **5,860** CITATIONS
SEE PROFILE

Yexiang Tong
Sun Yat-Sen University
297 PUBLICATIONS **8,173** CITATIONS
SEE PROFILE

Available from: Dai-Bin Kuang
Retrieved on: 01 February 2016

Controllable Electrochemical Synthesis of Hierarchical ZnO Nanostructures on FTO Glass

Xi-Hong Lu, Dong Wang, Gao-Ren Li, Cheng-Yong Su, Dai-Bin Kuang,* and Ye-Xiang Tong*

MOE Key Laboratory of Bioinorganic and Synthetic Chemistry, School of Chemistry and Chemical Engineering, Institute of Optoelectronic and Functional Composite Materials, Sun Yat-Sen University, Guangzhou 510275, P. R. China

Received: March 29, 2009; Revised Manuscript Received: June 16, 2009

Hierarchical ZnO hexagonal nanorods were successfully synthesized on fluorine-doped tin oxide (FTO) glass substrates via a simple electrodeposition from DMSO−H_2O solution. The formation process was studied in detail by observing time-dependent products, and an oriented attachment mechanism is suggested for the growth of these hierarchical hexagonal nanorods. The influence of reaction temperature and solvent on the morphologies of products was also investigated. Interestingly, the optical band gap of hierarchical ZnO nanorods can be tuned by simply changing the reaction temperature during the electrodeposition process.

Introduction

One-dimensional nanomaterials are fundamental to modern science and technology. During the past few decades, much effort has been devoted to preparing one-dimensional nanomaterials owing to their wide applications in electronic, optoelectronic, electrochemical, and electromechanical nanodevices.[1,2] Hierarchical assembly of one-dimensional nanostructures has more recently become the focus of intensive research because they combine the features of micrometer- and nanometer-scaled building blocks and exhibit unique properties different from those of one-dimensional structures. Moreover, they can be used as building units in nanodevices, which is crucial for the development of future nanodevices and nanotechnology.[3−5]

As an important functional oxide semiconductor, ZnO with a bang gap of about 3.37 eV and a large excitonic binding energy of about 60 meV at room temperature, has attracted extensive attention owing to its great potential applications in solar cells, UV photodetectors, photocatalysis, field emission, light-emitting diodes, etc.[6−10] One-dimensional ZnO nanostructures such as nanowires, nanorods, nanotubes, and nanobelts have been widely reported. Recently, some interesting hierarchical and complex nanostructures of ZnO including nails,[11] prism-like,[12] cones,[13] and paint-brush structures[14] have been synthesized by chemical vapor deposition, hydrothermal, and solvothermal methods. However, the previous reported methods generally need high temperature, high pressure, extended treatments or surfactants. It is still a challenge to develop a facile, mild and rapid synthesis method to prepare hierarchical ZnO nanostructures. To date, electrochemical deposition, which is acknowledged as a simple, quick, and economical method, has proved to be a powerful approach for the fabrication of one-dimensional ZnO nanostructures and shown its potential for the synthesis of hierarchical ZnO nanostructures.[15−17] For example, Xu et al.[17] have developed a two-step electrochemical deposition process to fabricate hierarchical ZnO nanostructures from aqueous solution, which involved the electrodeposition of ZnO crystals with different morphologies and the electrochemical epitaxial growth of oriented nanorods on the surfaces of the primary ZnO nanostructures. We also have successfully synthesized some hierarchical ZnO nanostructures such as ZnO dendritic structures, orientation-ordered ZnO nanorod bundles, and Tb^{3+}-doped ZnO nanorod bundles via electrochemical deposition in our previous studies.[18−20]

Dimethyl sulfoxide (DMSO), an important polar aprotic solvent, has been demonstrated to be a very useful solvent in fabricating metals and alloys due to its high dielectric constant, excellent solvating power and nontoxicity.[21,22] However, to the best of our knowledge, there are only a small number of reports on the preparation of ZnO via DMSO−H_2O system.[23−25] Herein, we present a one-step and controllable electrochemical route for large-scale synthesis of hierarchical ZnO nanorods on a transparent conductive substrate from DMSO−H_2O system. The present electrochemical route shows some significant advantages, such as rapid synthesis (1 h), low temperature (70−90 °C) and without surfactant, when compared to the previous reports which based on hydrothermal process.[26−30] Moreover, the hierarchical ZnO nanostructures could grow not only on glass coated with F-doped SnO_2 (FTO), but also on flexible polyethylene terephthalate (PET) substrates coated with indium-doped tin oxide (ITO), which will be of great potential use in optoelectronic applications, such as flexible displays and solar cells etc. The formation process of hierarchical ZnO nanorods was studied in detail by observing time-dependent products, and a possible growth mechanism based on oriented attachment was proposed. The optical properties of hierarchical ZnO nanorods were investigated as well. Furthermore, the morphology and size of ZnO can be readily controlled by adjusting the electrodeposition parameters such as reaction temperature and the concentration of DMSO.

Experimental Section

All reagents used were analytical grade and were used directly without any purification. The electrochemical deposition experiments were carried out in a three-electrode glass cell by galvanostatic electrolysis with a current density of 0.5 mA·cm^2. The reaction temperature was kept at 70 or 90 °C. During cathodic electrodepositon, a glass coated with F-doped SnO_2 (FTO) with a sheet resistance of 14 Ω/□ was used as the working electrode, a graphite rod of about 4.0 cm^2 was used as the auxiliary electrode, and a saturated calomel electrode (SCE) was used as the reference electrode that connect to the cell with

* Corresponding author. Tel.: +86 20 84110071. Fax: +86 20 84112245. E-mail: kuangdb@mail.sysu.edu.cn (D.B.K.); chedhx@mail.sysu.edu.cn (Y.X.T.).

10.1021/jp902834j CCC: $40.75 © 2009 American Chemical Society
Published on Web 07/09/2009

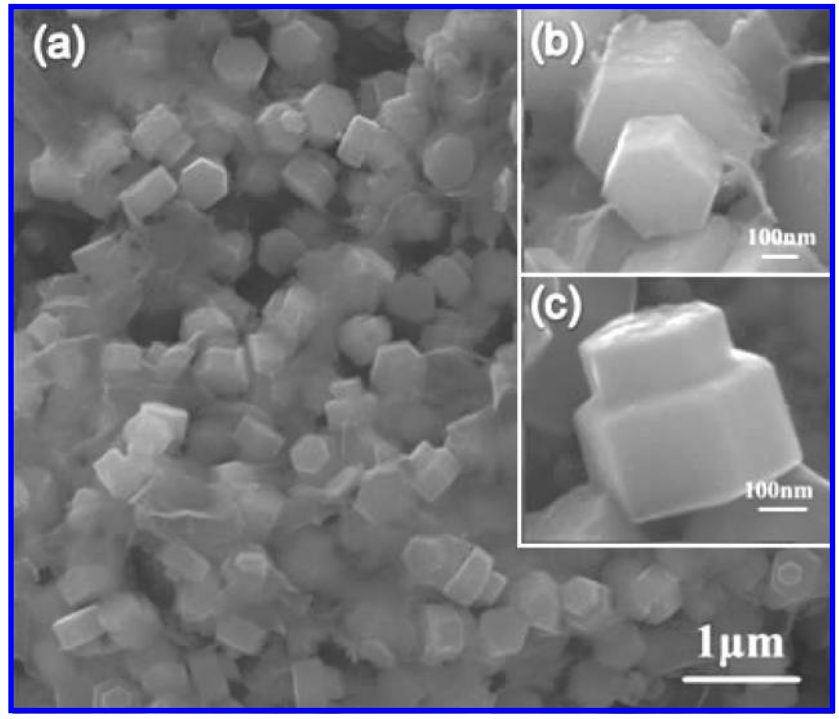

Figure 1. SEM images of the prepared ZnO in solution of 0.01 mol·L^{-1} $Zn(Ac)_2$ + 50% DMSO with a current density of 0.5 mA·cm^{-2} for 60 min at 70 °C.

a double salt bridge. The FTO glass was cleaned ultrasonically in distilled water, ethanol, and acetone and then rinsed in distilled water again before electrodeposition. The aqueous solution of DMSO was prepared using distilled water with different volume ratio.

The obtained deposits were characterized by field emission scanning electron microscope (FE-SEM, JSM-6330F), energy dispersive spectroscopy (EDS, FEI/Quanta 400), X-ray Diffractometer (XRD, D8 ADVANCE), transmission electron microscopy (TEM, JEM2010-HR). The optical properties of the ZnO nanostructures were measured with a UV−vis-NIR Spectrophotometer (UV, Shimadzu UV-3150) and a Combined Fluorescence Lifetime and Steady State Spectrometer (PL, EDINBURGH).

Results and Discussion

The electrochemical deposition of ZnO was performed using 0.01 mol·L^{-1} $Zn(Ac)_2$ in DMSO−H_2O (50 vol % DMSO:50 vol % H_2O, pH = 6.0) mixture solution with a current density of 0.5 mA·cm^{-2} for 60 min at 70 °C, and the typical SEM images are presented in Figure 1. It can be seen that hierarchical hexagonal ZnO nanorods were successfully synthesized on FTO glass substrates. Moreover, the hierarchical ZnO nanorods were fairly uniform and consisted of two well-defined hexagonal nanorods with different size. The diameter and length of the primary hexagonal nanorods are estimated to be 430 and 240 nm while those of the secondary hexagonal nanorods are 260 and 130 nm, respectively. It can be seen there are some nanoparticles on the surface of the hierarchical nanorods as shown in higher magnification SEM image in Figure S1 (see Supporting Information). The morphology of the hierarchical nanorods can be further modified by adjusting the electrochemical deposition temperature. When the growth temperature was increased to 90 °C, the size and morphology yield of hierarchical ZnO nanorods were dramatically increased as shown in Figure 2. Figure 2c is a magnified SEM image of ZnO hexagonal nanorods, revealing that the hierarchical ZnO nanorod consists of many nanoparticles (also see the higher magnification SEM image shown in Figure S2).

The chemical composition of the product from electrochemical deposition was characterized by EDS, and the representative EDS pattern of a hierarchical nanorods sample is shown in Figure 3a, revealing the presences of Zn and O in the sample. Figure 3b (black line) shows the X-ray diffraction (XRD) pattern of hierarchical nanorods obtained at 70 °C, and all the diffraction peaks can be perfectly indexed to a hexagonal wurtzite structure of ZnO (JCPDS: 36−1451) with lattice constants a = 3.25 Å and c = 5.207 Å. The XRD pattern of hierarchical nanostructures obtained at 90 °C (Figure 3b, red line) also can be indexed as a hexagonal wurtzite structure, but the intensity of the diffraction peaks is more than those of the deposits obtained at 70 °C. The sharp and intense diffraction peaks indicate that the deposit is highly crystalline.

The morphology and structure of hierarchical ZnO nanorods were further characterized by TEM. Figure 4a is a typical TEM image of the sample obtained at 70 °C, which shows the hierarchical ZnO nanorods were made up of two short hexagonal nanorods with different size. The selective area electron diffraction (SAED) pattern (inset in Figure 4a) recorded from the juncture of hierarchical nanorods, indicates the hierarchical ZnO nanorods are single crystalline with a hexagonal-wurtzite structure and the two hexagonal nanorods have the same crystallographic orientation. The HRTEM image (Figure 4b) of the top of a secondary nanorod (from the marked part by a white circle in Figure 4a) discloses a lattice fringe spacing of 0.52 nm, corresponding to the (001) lattice spacing of the wurtzite structure of ZnO. The corresponding fast Fourier transmission (FFT) pattern also confirms the nanorod has a hexagonal-wurtzite structure. Figure 4c displays the HRTEM image and the fast Fourier transmission (FFT) pattern of the primary nanorod (marked by a white rectangle in Figure 4a), showing that nanorod is single crystalline. The lattice fringe

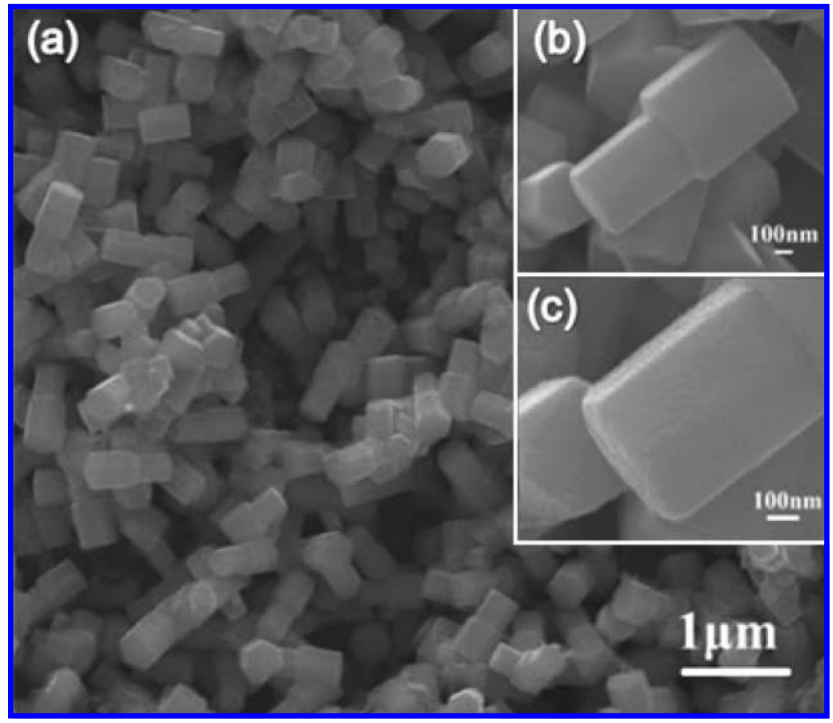

Figure 2. SEM images of the prepared ZnO in solution of 0.01 mol·L^{-1} $Zn(Ac)_2$ + 50% DMSO with a current density of 0.5 mA·cm^{-2} for 60 min at 90 °C.

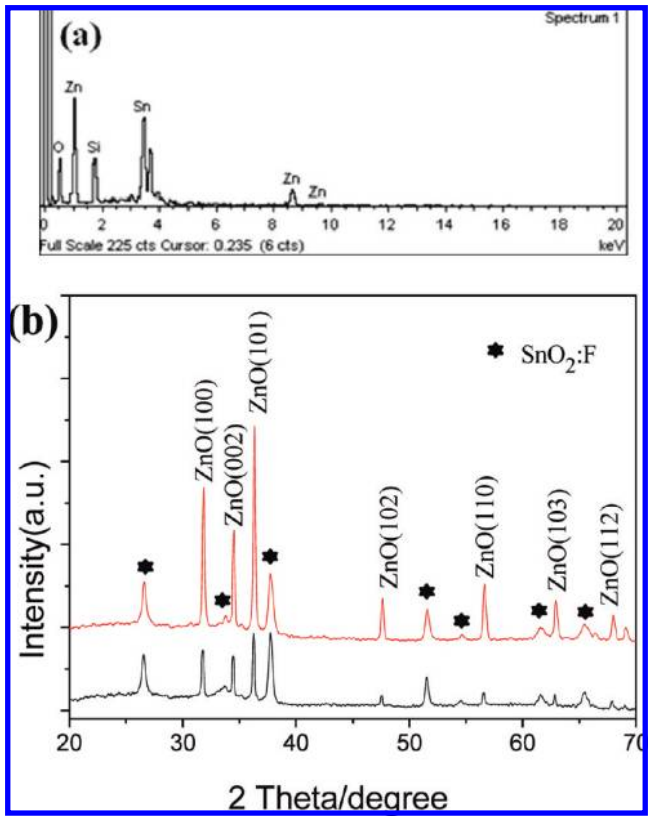

Figure 3. (a) EDS spectrum and (b) XRD patterns of hierarchical ZnO nanohexagons obtained at 70 °C (black line) and 90 °C (red line).

spacing is determined to be 0.26 nm, which is closed to the d value of the (002) lattice spacing of ZnO in the wurtzite phase. Based on these results, we can conclude that the two nanorods are single crystalline and the structures of hierarchical nanorods are uniform. Moreover, a similar results were obtained by analyzing the TEM and HRTEM of the product prepared in solution of 0.01 mol·L^{-1} $Zn(Ac)_2$ + 50%DMSO with a current density of 0.5 mA·cm^{-2} for 60 min at 90 °C. The typical TEM and HRTEM images of hierarchical ZnO nanostructures obtained at 90 °C are presented in Figure 5. There are abundant nanoparticles on the surface of the hierarchical nanohexagon as shown in Figure 5a. The HRTEM image of the secondary nanorod (marked by a white circle in Figure 5a) shows a lattice fringe spacing of 0.52 nm which is in good agreement with the (001) lattice spacing of ZnO in wurtzite phase, implying a good crystallinity (Figure 5b). The corresponding FFT pattern (inset in Figure 5b) further proves that the nanorod is single crystalline. Figure 5c shows the HRTEM image and FFT pattern recorded from the juncture of two coupled hexagonal nanorods (marked by a white rectangle in Figure 5a). The HRTEM image clearly discloses that the two hexagonal nanorods have parallel (001) lattice fringes, which reveals they have the same crystallographic orientation. According to the corresponding FFT pattern (inset in Figure 5c), it implies the hexagonal nanorods grow along (001) direction to form hierarchical nanostructures.

To gain insight into the growth mechanism of the hierarchical ZnO nanorods, the formation process of hierarchical ZnO nanorods was investigated using different electrodepositon times while monitored by SEM. Figure 6a-d shows a process of morphology evolution of hierarchical ZnO nanorods at various stages. As shown in Figure 6a, ZnO nanorods with well-defined hexagonal structure were first formed on the FTO glass substrate when the reaction time was 20 min. It is noteworthy that the surface of the nanorod was coated with large numbers of nanoparticles, implying these nanoparticles will be further developed into the final nanorods by oriented attachment. In order to decrease the surface energy, it is well-known that the nanoparticles will spontaneously aggregate through combining with adjacent nanoparticles with the same crystallographic orientation.[31−34] The TEM image in Figure 6g displays that the nanorod is hexagonal with the size of about 500 nm in diameter. The corresponding SAED pattern, as illustrated in Figure 6h,

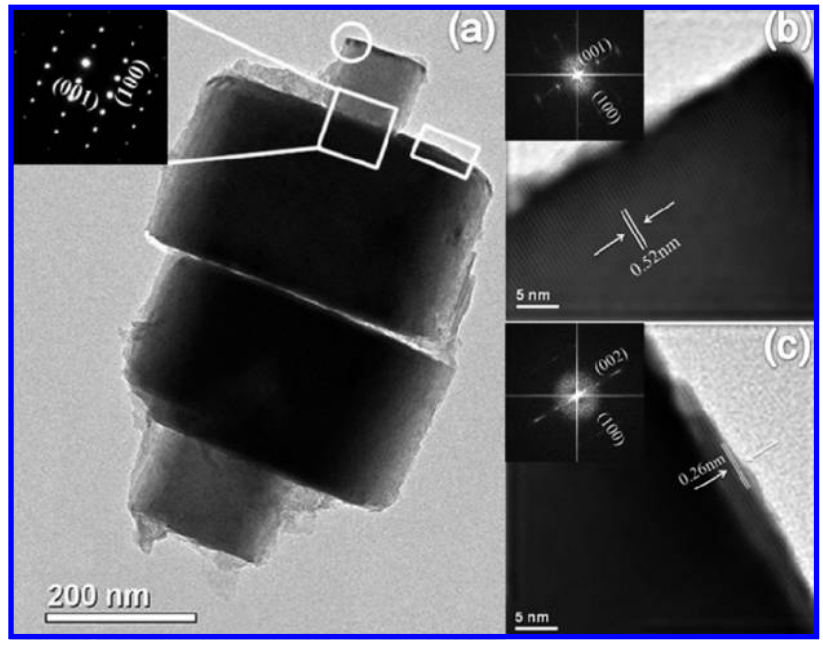

Figure 4. (a) TEM image of the prepared ZnO in solution of 0.01 mol·L^{-1} $Zn(Ac)_2$ + 50% DMSO with a current density of 0.5 mA·cm^{-2} for 60 min at 70 °C, the inset is the SAED pattern recorded from the juncture of hierarchical nanorod (marked by a white square); (b) HRTEM image of the top of secondary nanorod (marked by a white circle in a) and its corresponding FFT pattern; (c) HRTEM image of primary nanorod (marked by a white rectangle in a) and its corresponding FFT pattern.

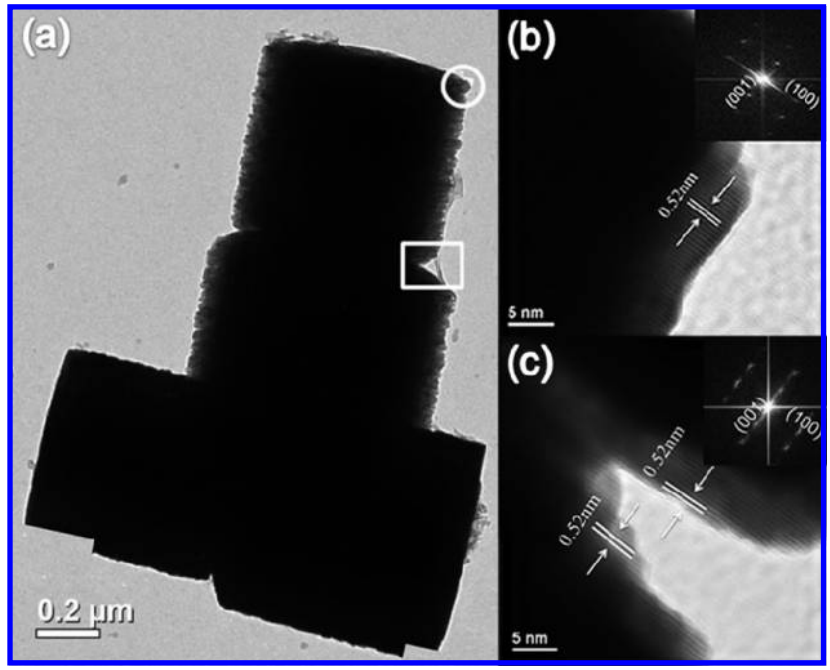

Figure 5. (a) TEM image of the prepared ZnO in solution of 0.01 mol·L^{-1} $Zn(Ac)_2$ + 50% DMSO with a current density of 0.5 mA·cm^{-2} for 60 min at 90 °C; (b) HRTEM image of the top of hierarchical nanorod (marked by a white circle in a) and the corresponding FFT pattern; (c) HRTEM image of the juncture of two coupled hexagonal nanorods (marked by a white rectangle in a) and the corresponding FFT pattern.

demonstrates the nanorod is single crystal. The side surfaces parallel to the *c*-axis are the $(10\bar{1}0)$, $(1\bar{1}00)$, and $(01\bar{1}0)$ planes, which are six crystallographically equivalent planes. As the reaction time increases to 30 min, the hierarchical ZnO nanorods began to be formed. It is observed from Figure 6b that a secondary hexagonal nanorod with small size grew on the surface of initially formed nanorods. With the prolongation of electrodeposition time, e.g., from 45 to 240 min, hierarchical ZnO nanorods further grew along both long and short axes resulting in a larger size of the ZnO nanorods, shown in Figure 6c,d. A control experiment was performed to investigate the effect of the electrodeposition on the ZnO morphology. Figure 6e,f shows the SEM images of the sample prepared in a solution of 0.01 mol·L^{-1} $Zn(Ac)_2$ + 50% DMSO at 70 °C for 60 min without electrochemical deposition process. Here no hierarchical nanorods were formed but rather some short hexagonal rods with a wide size distribution. Hence, it discloses the electrochemical process is crucial for the growth of hierarchical nanorods.

On the basis of the above results, it can be seen that the formation of hierarchical ZnO nanorods is probably dominated by oriented attachment. Herein, we propose a possible formation

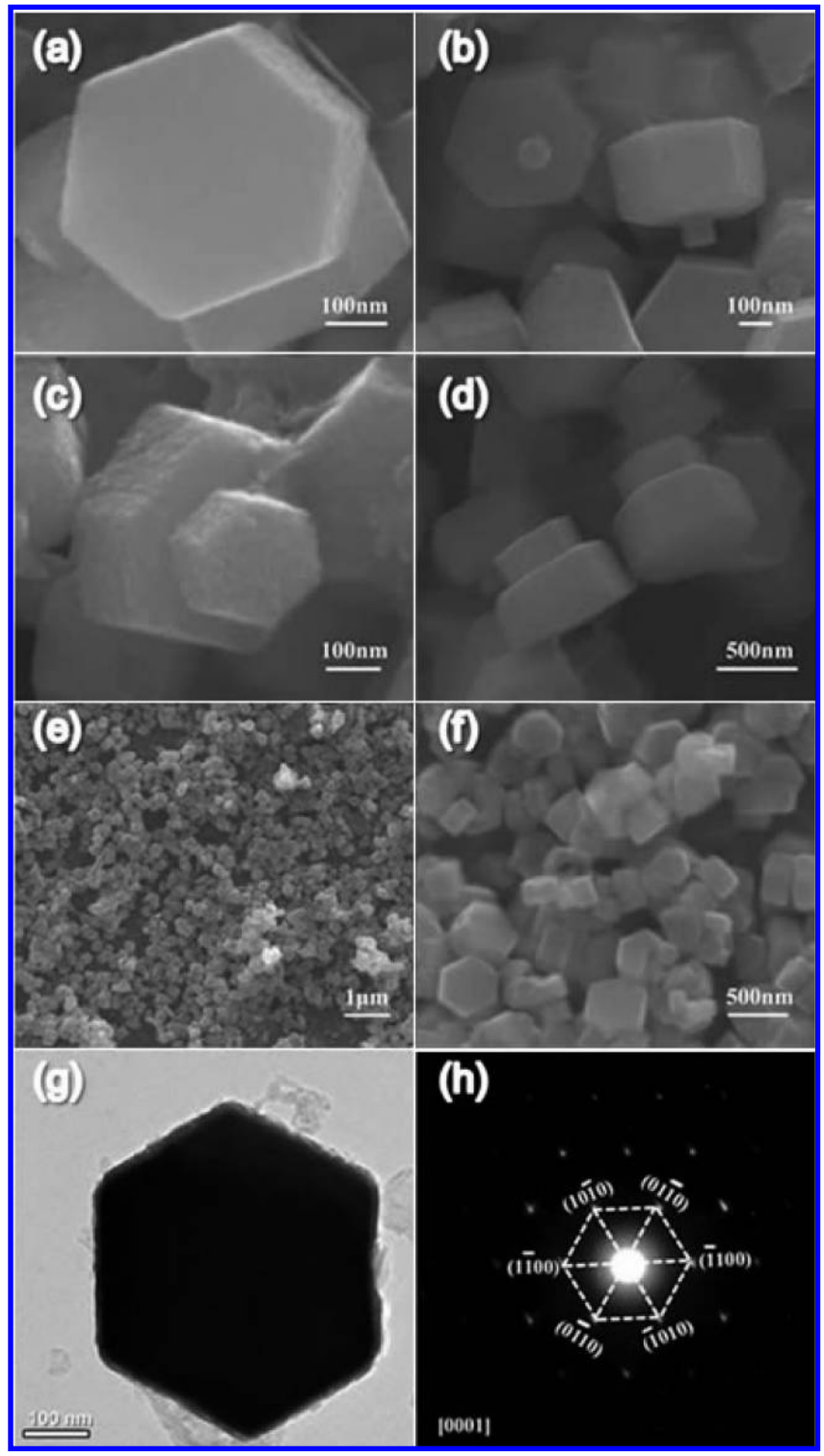

Figure 6. Time-dependent evolution of hierarchical ZnO hexagonal nanorods prepared in solution of 0.01 mol·L^{-1} $Zn(Ac)_2$ + 50% DMSO with a current density of 0.5 mA·cm^{-2} at different growth stages: (a) 20 min; (b) 30 min; (c) 45 min; (d) 240 min. (g, h) TEM image and SAED of nanorods for 20 min; (e, f) SEM images of the sample prepared in solution of 0.01 mol·L^{-1} $Zn(Ac)_2$ + 50% DMSO at 70 °C for 60 min without electrochemical deposition process.

mechanism of hierarchical ZnO hexagonal nanorods. The schematic illustration of the whole formation mechanism of hierarchical ZnO hexagonal nanorods is shown in Figure 7. The whole evolution process can be described as follows: At the beginning of electrodeposition, the concentration of the building blocks of ZnO gradually increases and produce ZnO nuclei as seeds for further growth. Then, these ZnO nuclei aggregate to form nanoparticles. Secondary, these nanoparticles self-assemble to hexagonal nanorods based on oriented attachment mechanism. It is well-known that the hexagonal wurtzite ZnO has two polar planes, i. e., the (001) and (00$\bar{1}$). The two polar planes have high surface energy and are metastable, which can absorb more new ZnO species than the nonpolar planes (six side surfaces parallel to the *c*-axis) and promote the anisotropic growth along the ± (001) direction. In addition, due to the surface energy of different crystallographic planes following the sequence (001)

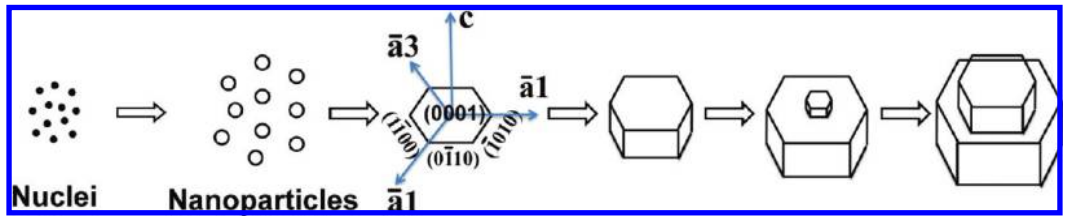

Figure 7. Schematic illustration of the formation mechanism of hierarchical ZnO hexagonal nanorods.

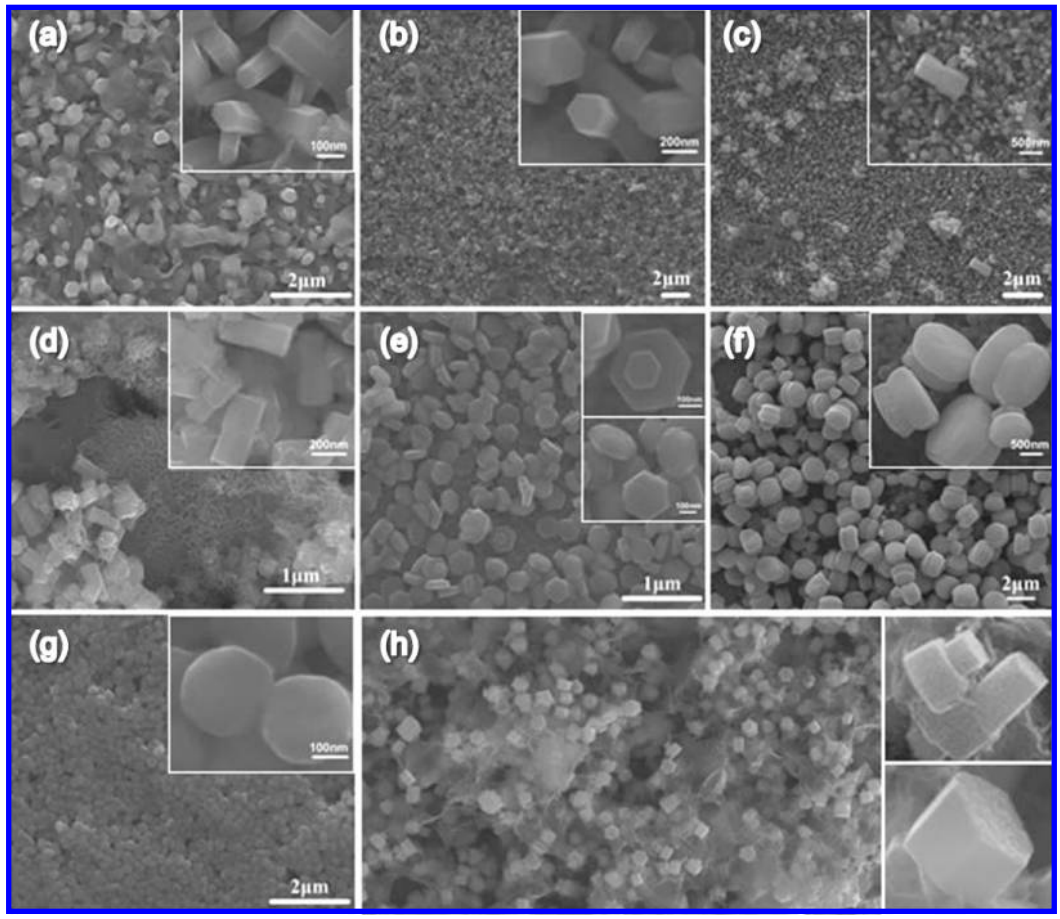

Figure 8. SEM images of the prepared ZnO in solution of 0.01 mol·L^{-1} $Zn(Ac)_2$ + (a) 0, (b) 10%, (c) 20%, (d) 40%, (e) 70%, (f) 80%, and (g) 90% DMSO with a current density of 0.5 mA·cm^{-2} for 60 min at 70 °C. (h−j) SEM images of the prepared ZnO on ITO-coated PET substrate in solution of 0.01 mol·L^{-1} $Zn(Ac)_2$ + 50% DMSO with a current density of 0.5 mA·cm^{-2} for 60 min at 70 °C.

> (101) > (100) in wurtzite ZnO, the growth rate of the (001) plane is the fastest.[16,35−37] Therefore, one-dimensional ZnO nanostructures such as nanotubes[16] and nanorods[32] will be obtained when they grow along the (001) direction. It has been reported that the hexagonal nanorods were formed when the growth along the (001) direction was suppressed by chemical surface modification in solution.[38−40] In our case, the growth rate of the (001) direction may be suppressed by absorbing a mass of DMSO polar molecules. Then the nanoparticles were self-assembled by sharing a common crystallographic orientation along the (0001) and the six side surfaces parallel to the *c*-axis to form hexagonal nanorods. In the following steps, the hexagonal nanorods further grew and attached a small size secondary hexagonal nanorods on the (001) plane to form hierarchical nanorods. This process can be attributed to oriented attachment and was already confirmed by HRTEM observations shown in Figure 4 and 5. HRTEM results proved that the two hexagonal nanorods are self-assembled by sharing the (001) plane in Figure 5c. According to the above analysis, it is considered that the electrostatic interactions between the two polar planes ± (001) and electric field during the electrodeposition process are the probable driving forces for the self-assembly formation process of the hierarchical secondary ZnO nanorods. However, third or more hierarchical ZnO structures were not found, even though the reaction time increased to 240 min (Figure 6d). It is probably due to the fact that the driving force is too weak to overcome the geometrical and physical limitation deriving from the hierarchical secondary ZnO to form three or more hierarchical structures.[41−43] As a result, the second hierarchical ZnO nanorods will grow up.

Based on the above discussions, DMSO may have an important influence on the ZnO morphology. Hence, we systematically investigated the effect of different DMSO concentrations on the ZnO morphology. Figure 8 shows the SEM images of the products prepared at various concentrations of DMSO with a current density of 0.5 mA·cm^{-2} for 60 min at 70 °C. The pH value of the solution increases from 5.5 to 6.5 with increasing concentration of DMSO from 0 to 90%. A typical pH value of the solution containing 50% DMSO is 6.0. When the DMSO was less than 30% in volume, the product

was dominated by the presence of hexagonal nanorods, as shown in Figure 8a,c. Hierarchical ZnO hexagonal nanorods were already formed while the concentration of DMSO was 40% in Figure 8d. When the concentration of DMSO was increased to 50%, the final product was hierarchical ZnO hexagonal nanorods, and the morphology was close to unity (Figure 1). With the further increase of the DMSO concentration, the morphology of the dominating product changed from hierarchical hexagonal nanorods, hierarchical irregular nanorods to irregular nanorods (Figure 8e−g). Hence, the morphology of ZnO products can be readily tuned by optimizing the concentration of DMSO. Moreover, we have successfully fabricated ZnO nanorods on the flexible substrates (PET) coated with indium-doped tin oxide (ITO) via electrodeposition in solution of 0.01 mol·L^{-1} $Zn(Ac)_2$ + 50% DMSO with a current density of 0.5 mA·cm^{-2} for 60 min at 70 °C. Figure 8h−j shows the SEM images of well-defined hexagonal simple and hierarchical ZnO nanorods on the flexible ITO-PET substrates. It implies that the present electrodeposition fabrication of ZnO nanorods can be easily extended to other conductive substrates, which is a potential candidate for various practical applications.

The electrochemical deposition reactions to fabricate ZnO nanostructures are proposed as follows

$$2H_2O + 2e^- \rightarrow H_2 + 2OH^- \qquad \varphi^{\Phi} = -0.828\ V \tag{1}$$

$$4OH^- \rightarrow O_2 + 2H_2O + 4e^- \qquad \varphi^{\Phi} = 0.401\ V \tag{2}$$

$$Zn^{2+} + 4OH^- \rightarrow Zn(OH)_4^{2-} \tag{3}$$

$$Zn(OH)_4^{2-} \rightarrow ZnO + 2H_2O \tag{4}$$

At first, H_2O is electrolyzed and produce OH^- ions on the cathode. Then, the OH^- will react with Zn^{2+} to form $Zn(OH)_4^{2-}$ ions via eq 3, which is a rapid reaction process. Finally, the formed $Zn(OH)_4^{2-}$ ions will decompose to produce ZnO on the substrate at 70 °C via eq 4. During the reaction process, DMSO not only plays a role as solvent but also as reactant. DMSO can produce OH^- ions and accommodate the concentration of OH^- through hydrolysis in solution, according to the follow equilibrium:[44]

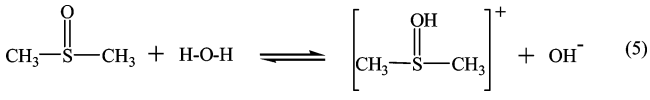

(5)

The concentration of OH^- is a key factor to form $Zn(OH)_4^{2-}$, which is crucial for nucleation and growth of ZnO. In addition, the physicochemical properties of solvent such as the surface tension, dielectric constant, viscosity, and saturated vapor pressure have been reported to be key parameters in controlling nanomaterials formation. For example, Geonel et al.[25] proved that the solvent basicity and the interaction of DMSO−H_2O play crucial roles in the formation of ZnO nanoparticles. The actual role of DMSO on ZnO nanostructures formation is still not clear and needs further investigation.

The optical properties of hierarchical ZnO nanorods were further examined by using UV−vis−NIR spectroscopy. Figure 9a shows the transmittance (*T*%) spectra of the as-synthesized

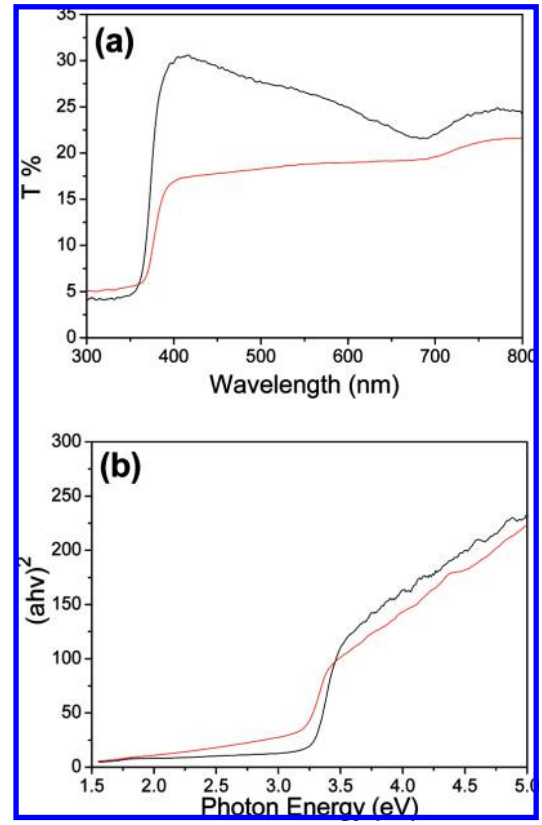

Figure 9. (a) Optical transmittance (*T*%) spectra of the ZnO nanorods prepared in solution of 0.01 mol·L^{-1} $Zn(Ac)_2$ + 50% DMSO with a current density of 0.5 mA·cm^{-2} for 60 min at 70 °C (black line) and 90 °C (red line). (b) The corresponding band gaps are estimated from the zero-crossing values obtained by extrapolation of a linear fit to the rising edges of the respective $[(-\ln T)h\nu]^2$ vs $h\nu$, 70 °C (black line) and 90 °C (red line).

ZnO nanorods deposited at 70 and 90 °C. We noted that the *T*% from the hierarchical nanorods obtained both at 70 and 90 °C is rather low. The low transmittance of the present hierarchical ZnO nanorods suggests that the incident light is significantly blocked due to the strong scattering or reflection within the ZnO films made from submicrometer-sized ZnO rods with dimensions comparable to the wavelength of incident light.[45] According to the data of the *T*% spectra, the optical band gaps (E_g) of ZnO can be estimated by using the conventional Tauc equation:[46]

$$\alpha h\nu = A(h\nu - E_g)^{n/2} \tag{6}$$

Here α (α = −ln *T*) is the absorption coefficient, $h\nu$ is the photon energy, A is a constant. As a direct band gap semiconductor, the optical band gap (E_g) of ZnO can be estimated by the zero crossing of the rising edge of the $(\alpha h\nu)^2$ vs $h\nu$ curve, as shown in Figure 9b. The estimated E_g of nanorods obtained at 70 and 90 °C are about 3.19 and 3.02 eV, respectively. The two values are slightly smaller than that of bulk ZnO (3.37 eV). It is well-known that the impurities in ZnO nanostructures can adjust the crystal structures and cause the change of properties. ZnO doping with different transition metal ions is an effective approach to tune up the optical band gap of ZnO.[37−48] However, in our present case, any impurities such as hydroxide could not be observed in the electrodeposition products by analyzing the EDS, XRD, and TEM. Hence, the influence of impurities on the optical band gap can be negative. Recently, modulating the band gap of ZnO via electrodeposition has proved to be

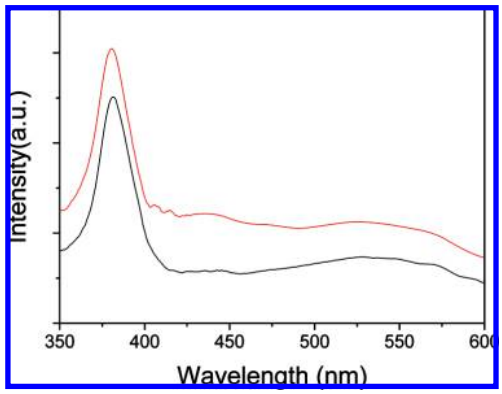

Figure 10. (a) PL spectra of the as-synthesized ZnO nanorods in solution of 0.01 mol·L^{-1} $Zn(Ac)_2$ + 50% DMSO with a current density of 0.5 mA·cm^{-2} for 60 min at 70 (black line) and 90 °C (red line).

available, and a similar red shift has been reported for electrodeposited ZnO films from $Zn(NO_3)_2$ solution by Anthony et al.[49−51] They found that the optical band gap of ZnO nanowire arrays grown from $Zn(NO_3)_2$ solution in the presence of hydrogen peroxide showed redshift, while blueshift was observed for the products grown from $Zn(NO_3)_2$ solution in the absence of hydrogen peroxide. In our experiment, O_2 was produced on the anode which increased the concentration of O_2 dissolved in solution, resulting in zinc defects variation in nanorods. Therefore, we considered the zinc defects in the nanorods may be responsible for redshift of ZnO band gap.

The room temperature photoluminescence spectra of the as-synthesized ZnO nanorods deposited at 70 and 90 °C utilizing the excitation wavelength at 325 nm is shown in Figure 10. The two samples exhibit a strong ultraviolet UV emission peak and a weak visible emission peak. The UV peak at about 380 nm is attributed to the excitonic recombination of the near-band-edge emission. The weak visible broad peak at about 470−570 nm region is ascribed to the intrinsic defect centers such as zinc vacancy, oxygen vacancy.[52,53] The intensity ratio of the UV emission and the visible emission of the ZnO nanorods deposited at 70 and 90 °C is ca. 3.37 and 2.69, respectively. Thus, it suggests the crystal quality of ZnO nanorods obtained at 70 °C is better than that obtained at 90 °C, which is consistent with the above UV−vis data. As it is known, nucleation and growth will accelerate with increasing temperature, and the rapid nucleation and growth processes are beneficial to forming crystal defects.

Conclusion

In summary, we successfully synthesized hierarchical ZnO hexagonal nanorods by a simple electrochemical reaction. The formation of high-quality hierarchical ZnO nanorods can be ascribed to an oriented attachment mechanism. We proposed a formation mechanism. The concentration of DMSO plays a significant role in the formation and morphology of ZnO. In addition, the optical band gaps of hierarchical ZnO nanorods exhibit a red shift because of defects in the structure. The present study provides a new scheme to fabricate hierarchical ZnO nanostructures on any conductive substrates which is of potential use in solar cells and flexible displays.

Acknowledgment. This work was supported by the Natural Science Foundations of China (Grant Nos. 20873184, 20873183) and the Natural Science Foundations of Guangdong Province (Grant Nos. 2008B010600040, 8151027501000030).

Supporting Information Available: Higher magnification SEM images of the products with hierarchical ZnO hexagonal nanorods prepared at 70 and 90 °C. SEM images of samples prepared after 240 min electrodeposition. This material is available free of charge via the Internet at http://pubs.acs.org.

References and Notes

(1) Xia, Y. N.; Yang, P. D.; Sun, Y. G.; Wu, Y. Y.; Mayers, B.; Gates, B. *Adv. Mater.* **2003**, *15*, 354.
(2) Kar, S.; Pal, B. N.; Chaudhuri, S.; Chakravorty, D. *J. Phys. Chem. B* **2006**, *110*, 4605.
(3) Gao, X. F.; Jiang, L. *Nature* **2004**, *432*, 36.
(4) Pan, Z. W.; Mahurin, S. M.; Dai, S.; Lowndes, D. H. *Nano Lett.* **2005**, *5*, 723.
(5) Wang, Z. L.; Song, J. H. *Science* **2006**, *312*, 242.
(6) Zhang, Q. F.; Chou, T. P.; Russo, B.; Jenekhe, S. A.; Cao, G. Z. *Angew. Chem., Int. Ed.* **2008**, *47*, 2402.
(7) Wang, Z. L. *J. Phys.: Condens. Matter.* **2004**, *16*, R829.
(8) Soci, C.; Zhang, A.; Xiang, B.; Dayeh, S. A.; Aplin, D. P. R.; Park, J.; Bao, X. Y.; Lo, Y. H.; Wang, D. *Nano Lett.* **2007**, *7*, 1003.
(9) Bao, J. M.; Zimmler, M. A.; Capasso, F.; Wang, X. W.; Ren, Z. F. *Nano Lett.* **2006**, *6*, 1719.
(10) Lu, F.; Cai, W. P.; Zhang, Y. G. *Adv. Funct. Mater.* **2008**, *18*, 1047.
(11) Lao, J. Y.; Wen, J. G.; Ren, Z. F. *Nano Lett.* **2002**, *2*, 1287.
(12) Wu, Q. Z.; Chen, X.; Zhang, P.; Han, Y. C.; Chen, X. M.; Yan, Y. H.; Li, S. P. *Cryst. Growth Des.* **2008**, *8*, 3010.
(13) Lu, F.; Cai, P. W.; Zhang, Y. G. *Adv. Funct. Mater.* **2008**, *18*, 1047.
(14) Kar, S.; Santra, S. *J. Phys. Chem. C* **2008**, *112*, 8144.
(15) Cheng, J.; Aichele, L. C.; Lux-Steiner, M. C. *Appl. Phys. Lett.* **2008**, *92*, 161906.
(16) Tang, Y. W.; Luo, L. J.; Chen, Z. G.; Jiang, Y.; Li, B. H.; Jia, Z. Y.; Xu, L. *Electrochem. Commun.* **2007**, *9*, 289.
(17) Xu, L. F.; Chen, Q. W.; Xu, D. S. *J. Phys. Chem. C* **2007**, *111*, 11560.
(18) Li, G. R.; Lu, X. H.; Qu, D. L.; Yao, C. Z.; Zheng, F. L.; Bu, Q.; Dawa, C. R.; Tong, Y. X. *J. Phys. Chem. C* **2007**, *111*, 6678.
(19) Li, G. R.; Dawa, C. R.; Bu, Q.; Lu, X. H.; Ke, Z. H.; Hong, H. E.; Yao, C. Z.; Liu, P.; Tong, Y. X. *Electrochem. Commun.* **2007**, *9*, 863.
(20) Li, G. R.; Lu, X. H.; Su, C. Y.; Tong, Y. X. *J. Phys. Chem. C* **2008**, *112*, 2927.
(21) Tan, S. Z.; Yuan, D. S.; Liu, Y. L. *Mater. Lett.* **2006**, *60*, 2055.
(22) Li, G. R.; Chen, j. C.; Chen, L. P.; Liu, P.; Liu, G. K.; Tong, Y. X. *Electrochem. Solid-State Lett.* **2006**, *9*, C102.
(23) Liu, Y. L.; Liu, Y. C.; Zhang, J. Y.; Lu, Y. M.; Shen, D. Z.; Fan, X. W. *J. Cryst. Growth* **2006**, *290*, 405.
(24) Mollar, M.; Tortosa, M.; Casasu, R.; Mar, B. *Microelectr. J.* **2009**, *40*, 276.
(25) Geonel, R. G.; Patricia, S. J.; L.Rendon, V.; Jozsef, N.; Imre, D.; Diaz, D. *J. Phys. Chem. B* **2003**, *107*, 12597.
(26) Wang, B. G.; Shi, E. W.; Zhong, W. Z. *Cryst. Res. Technol.* **1998**, *33*, 937.
(27) Zhang, H.; Yang, D.; Li, D.; Ma, X.; Li, S.; Que, D. *Cryst. Growth Des.* **2004**, *5*, 547.
(28) Wang, R. H.; Xin, J. H.; Tao, X. M. *Inorg. Chem.* **2005**, *44*, 3926.
(29) Yu, Q. J.; Yu, C. L.; Yang, H. B.; Fu, W. Y.; Chang, L. X.; Xu, J.; Wei, R. H.; Li, H. D.; Zhu, H. Y.; Li, M. H.; Zou, G. T. *Inorg. Chem.* **2007**, *46*, 6204.
(30) Zhao, W.; Song, X. Y.; Chen, G. Z.; Sun, S. X. *Cryst. Res. Technol.* **2009**, *44*, 373.
(31) Banfield, J. F.; Welch, S. A.; Zhang, H.; Ebert, T. T.; Penn, R. L. *Science* **2000**, *289*, 751.
(32) Li, P.; Liu, H.; Zhang, Y. F.; Wei, Y.; Wang, X. K. *Mater. Chem. Phys.* **2007**, *106*, 63.
(33) Li, Y. J.; Wang, C. Y.; Lu, M. Y.; Li, K. M.; Chen, L. J. *Cryst. Growth Des.* **2008**, *8*, 2598.
(34) Jia, B. P.; Gao, L. *Cryst. Growth Des.* **2008**, *8*, 1372.
(35) Zhang, J. H.; Liu, H. Y.; Wang, Z. L.; Ming, N. B.; Li, Z. R.; Biris, A. S. *Adv. Funct. Mater.* **2007**, *17*, 3897.
(36) Liu, Y. L.; Liu, Y. C.; Zhang, J. Y.; Lu, Y. M.; Shen, D. Z.; Fan, X. W. *J. Cryst. Growth* **2006**, *290*, 405.
(37) Pradhan, D.; Leung, K. T. *J. Phys. Chem. C* **2008**, *112*, 1357.
(38) Tian, Z.; Voigt, J. A.; Liu, J.; Mchenzie, B.; Mcdermott, M. J.; Rodriguez, M. A.; Konishi, H.; Xu, H. *Nat. Mater.* **2003**, *21*, 821.
(39) Xu, C. X.; Sun, X. W.; Dong, Z. L.; Yu, M. B. *Appl. Phys. Lett.* **2004**, *85*, 3878.
(40) Li, F.; Ding, Y.; Gao, P. X.; Xin, X. Q.; Wang, Z. L. *Angew. Chem., Int. Ed.* **2004**, *43*, 5238.
(41) Moldovan, D.; Yamakov, V.; Wolf, D.; Phillpot, S. R. *Phys. ReV. Lett.* **2002**, *89*, 206101.
(42) Ribeiro, C.; Lee, E. J. H.; Longo, E.; Leite, E. R. *ChemPhysChem* **2005**, *6*, 690.

(43) Liu, J. P.; Huang, X. T.; Li, Y. Y.; Sulieman, K. M.; He, X.; Sun, F. L. *Cryst. Growth Des.* **2006**, *6*, 1690.
(44) Calligaris, M.; Carugo, O. *Coord. Chem. Rev.* **1996**, *153*, 83.
(45) Chen, D. H.; Huang, F. Z.; Cheng, Y. B.; Caruso, R. A. *Adv. Mater.* **2009**, *21*, 1.
(46) Tauc, J.; Menth, A. *J. Non-Cryst. Solids* **1972**, *8*−*10*, 569.
(47) Li, G. R.; Lu, X. H.; Su, C. Y.; Tong, Y. X. *J. Phys. Chem. C* **2008**, *112*, 2927.
(48) Wang, Y. S.; Thomas, P. J.; Brien, P. O. *J. Phys. Chem. B* **2006**, *110*, 21412.
(49) Anthony, S. P.; Lee, J. N.; Kima, J. K. *Appl. Phys. Lett.* **2007**, *90*, 103107.
(50) Jayakrishnan, R.; Hodes, G. *Thin Solid Films* **2003**, *440*, 19.
(51) Pradhan, D.; Leung, K. T. *J. Phys. Chem. C* **2008**, *112*, 1357.
(52) Dev, A.; Kar, S.; Chakrabarty, S.; Chaudhuri, S. *Nanotechnology* **2006**, *17*, 1533.
(53) Kar, S.; Dev, A.; Chaudhuri, S. *J. Phys. Chem. B* **2006**, *110*, 17848–17853.

JP902834J